A Multitarget Tracking Method for Estimating Carotid Artery Wall Motion from Ultrasound Sequences

Jan Dorazil*, Rene Repp*,†, Thomas Kropfreiter*,†, Richard Prüller†, Kamil Říha*, and Franz Hlawatsch*,†

*Department of Telecommunications, Brno University of Technology, Brno, Czech Republic
†Institute of Telecommunications, TU Wien, Vienna, Austria

Abstract—**Analyzing the motion of the wall of the common carotid artery (CCA) yields effective indicators for atherosclerosis. In this work, we introduce the use of multitarget tracking techniques for estimating the time-varying CCA radius from an ultrasound video sequence. We employ the joint integrated probabilistic data association (JIPDA) filter to track a set of "feature points" (FPs) located around the CCA wall cross section. Subsequently, we estimate the time-varying CCA radius via a nonlinear least-squares method and a Kalman filter. The application of the JIPDA filter is enabled by a linear state-space model describing the quasi-periodic movement of the FPs and the measurement extraction process. Simulation results using the Field II ultrasound simulation program show that the proposed multitarget tracking method can outperform a state-of-the-art method based on optical flow.**

Index Terms—**Atherosclerosis, common carotid artery, ultrasound video processing, speckle tracking, multitarget tracking, joint integrated probabilistic data association (JIPDA) filter.**

I. INTRODUCTION

Atherosclerosis is a major cause of death [1]. Effective indicators for atherosclerosis can be obtained from an analysis of the motion of the wall of the common carotid artery (CCA) [2], [3]. This paper presents a new methodology for estimating CCA wall motion from a B-mode ultrasound video sequence.

Most methods for estimating CCA wall motion are based on speckle tracking [4]. One of the first applications of speckle tracking to CCA wall motion estimation used block matching [5], [6], which is, however, affected by a phenomenon known as speckle decorrelation [5]. This issue was addressed by using a state-space model for the evolution of the reference block [7], [8] or for the movement of the artery [3], [9]. As an alternative to block matching, techniques based on optical flow [10] were proposed [11], [12]. A comparison of different speckle tracking techniques in [13] showed that a modified Lucas-Kanade algorithm outperforms other optical flow algorithms as well as block matching algorithms. The method proposed in [14] uses the modified Lucas-Kanade algorithm and performs an explicit feature drift compensation.

Here, we develop a new approach to speckle tracking that uses multitarget tracking techniques known from radar surveil-

lance [15]–[17]. We model the CCA wall cross section as a circle, and our goal is to estimate the time-varying circle radius from a B-mode ultrasound video sequence showing a transverse scan of the CCA. We use a particular multifeature tracking filter, the joint integrated probabilistic data association (JIPDA) filter [16], [17, Ch. 5], to track "feature points" (FPs) located around the CCA wall cross section. The time-varying CCA radius is then estimated by fitting a circle to the tracked FPs. The use of the JIPDA filter solves the problem of speckle decorrelation: any change in the speckle pattern is automatically detected and accounted for by removing disappeared FPs and initializing newly appeared FPs.

The main contributions of this work are (i) the introduction and development of the multifeature tracking methodology in medical image analysis; (ii) the establishment of a linear state-space model describing the quasi-periodic movement of the FPs and the measurement extraction process; and (iii) the embedding of the JIPDA filter in an overall method for CCA wall motion estimation (as summarized in Fig. 1). The paper is organized as follows. An overview of the proposed method is given in Section II. The system model underlying the method is developed in Section III. The method is described in Section IV. Finally, simulation results are presented in Section V.

II. METHOD OVERVIEW

The input to the proposed method is a B-mode ultrasound video sequence showing temporally successive transverse scans of the CCA. From the first video frame ($t = 1$), a rectangular region of interest that delimits the CCA wall transverse section is detected via the modified Viola-Jones detector proposed in [18]. To find the CCA wall, which is modeled as a circle, circle detection is performed by using the Hough transform [19] in the region of interest. This results in a preliminary CCA center point $\tilde{c} \in \mathbb{R}^2$ and a preliminary CCA radius $\tilde{r} > 0$. Subsequently, for all video frames ($t = 1, 2, \ldots$), our method consists of three parts, as visualized in Fig. 1 and discussed in the following.

Measurement extraction: At each frame time $t = 1, 2, \ldots$, measurements (points) $\boldsymbol{z}_t(j) \in \mathbb{R}^2$, $j = 1, \ldots, N'_t$ are detected within an annular search region by means of the Harris detector [20]. The annular search region is centered at $\hat{\boldsymbol{c}}_{t-1}$ (which was estimated at the previous frame time $t-1$ as described in
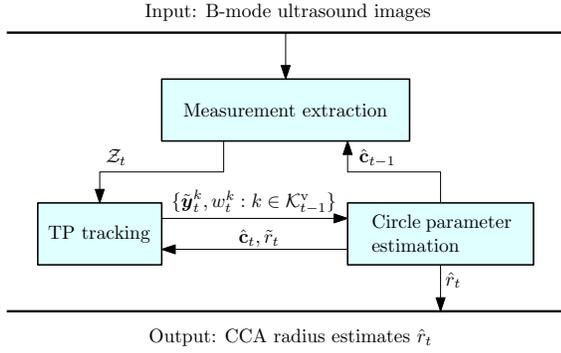
Fig. 1. Block diagram of the proposed method.

Section IV-C, except for $\hat{\boldsymbol{c}}_0$, which is equal to $\tilde{\boldsymbol{c}}$), and it has inner radius $\tilde{r}-\Delta r$ and outer radius $\tilde{r}+\Delta r$, with $\Delta r > 0$. The final number of measurements is chosen as $N_t = \min(N_t', N_{\max})$, where N_t' was determined by the detection procedure and $N_{\max}$ is a prespecified maximum number of measurements. The output of the measurement extraction stage is the set $\mathcal{Z}_t$ of those N_t measurements $\boldsymbol{z}_t(j)$ that achieve the highest quality in the sense defined in [20].

FP tracking: The measurement set $\mathcal{Z}_t$ constitutes the input to a FP tracking algorithm based on the JIPDA filter (see Section IV-A). A FP is a simplified single-point representation of a local configuration of strong scatterers in the monitored tissue, which yields a large response in the response map of the Harris detector [21, Ch. 9]. The JIPDA filter estimates (tracks) the positions $\boldsymbol{y}_t^k \in \mathbb{R}^2$ and existence probabilities $\hat{p}_t^k \in [0,1]$ of the FPs $k \in \mathcal{K}_t$ that are present at frame time t. Note that $\mathcal{K}_t$, the estimated set of FPs k, changes with time t. Based on the estimated FP existence probabilities and previously calculated *wall association beliefs* (WABs), a subset $\mathcal{K}_{t-1}^{\text{v}} \subseteq \mathcal{K}_{t-1}$ of "valid FPs" is selected (see Section IV-B).

Circle parameter estimation: The estimated positions of the valid FPs, $\tilde{\boldsymbol{y}}_t^k$ for $k \in \mathcal{K}_{t-1}^{\text{v}}$, are passed to the circle parameter estimation stage. This stage calculates new CCA circle parameter estimates $\hat{\boldsymbol{c}}_t$ and $\tilde{r}_t$ via a nonlinear weighted least-squares fit (see Section IV-C). These estimates are fed back to the FP tracking stage, where they are used to correct the current FP state estimates (see Section IV-D) and to calculate the WABs (see Section IV-F). Finally, the radius estimates $\tilde{r}_t$ are filtered by a Kalman filter. The resulting new radius estimates, denoted $\hat{r}_t$, are the output of the overall method.

III. SYSTEM MODEL

The proposed tracking method is based on a probabilistic "system model" that describes (i) the temporal variation of the FP radii r_t^k, $k \in \mathcal{K}_t$ and the evolution of the underlying FP states, and (ii) the measurement extraction process.

A. FP Radii, FP States, and FP Existence Variables

Besides the vector $\boldsymbol{y}_t^k \in \mathbb{R}^2$ representing the position of FP $k \in \mathcal{K}_t$ in Cartesian coordinates, we will also use the representation in polar coordinates, $\boldsymbol{y}_t^{k\star} \triangleq (r_t^k \ \theta_t^k)^{\text{T}}$, where the origin of the coordinate system is defined to be the current CCA center point $\boldsymbol{c}_t$. We note that $\boldsymbol{y}_t^k$ and $\boldsymbol{y}_t^{k\star}$ are related by

$$\boldsymbol{y}_t^k = \boldsymbol{c}_t + \phi^{-1}(\boldsymbol{y}_t^{k\star}), \qquad (1)$$

where $\phi^{-1}(\boldsymbol{y}_t^{k\star}) \triangleq \big(r_t^k \cos(\theta_t^k) \ \ r_t^k \sin(\theta_t^k)\big)^{\text{T}}$. The regularity of the heart beat manifests itself in an approximate periodicity of the radial movement of the FPs. Therefore, we model the time-dependence of the FP radius r_t^k by the superposition of M harmonic components [22, Ch. 11] with time-dependent coefficients, plus a slowly varying component s_t^k that captures *breathing artifacts* [14], i.e.,

$$r_t^k = \sum_{m=1}^{M} \big(a_{t,m}^k \cos(m\omega t) + b_{t,m}^k \sin(m\omega t)\big) + s_t^k. \qquad (2)$$

The fundamental frequency ω is estimated by a separate method, e.g., based on an electrocardiogram.

Extending [23], the *state* of FP $k \in \mathcal{K}_t$ at time t is now defined as the $(2M+2)$-dimensional random vector $\boldsymbol{x}_t^k \triangleq \big(\boldsymbol{a}_t^{k\text{T}} \ \boldsymbol{b}_t^{k\text{T}} \ s_t^k \ \theta_t^k\big)^{\text{T}}$, with $\boldsymbol{a}_t^k \triangleq (a_{t,1}^k \cdots a_{t,M}^k)^{\text{T}}$ and $\boldsymbol{b}_t^k \triangleq (b_{t,1}^k \cdots b_{t,M}^k)^{\text{T}}$. Here, the angle θ_t^k does not carry any information about the radial movement of the CCA, but it helps distinguish between individual FPs. The FP state $\boldsymbol{x}_t^k$ completely specifies the FP position $\boldsymbol{y}_t^{k\star}$ via

$$\boldsymbol{y}_t^{k\star} = \boldsymbol{H}_t \boldsymbol{x}_t^k, \qquad (3)$$

where $\boldsymbol{H}_t \triangleq \begin{pmatrix} \boldsymbol{h}_t^a & \boldsymbol{h}_t^b & 1 & 0 \\ \boldsymbol{0} & \boldsymbol{0} & 0 & 1 \end{pmatrix}$ with $\boldsymbol{h}_t^a \triangleq \big(\cos(\omega t) \ \cos(2\omega t) \cdots \cos(M\omega t)\big)$ and $\boldsymbol{h}_t^b \triangleq \big(\sin(\omega t) \ \sin(2\omega t) \cdots \sin(M\omega t)\big)$. We model the temporal evolution of each FP state $\boldsymbol{x}_t^k$ by a random walk, i.e.,

$$\boldsymbol{x}_t^k = \boldsymbol{x}_{t-1}^k + \boldsymbol{v}_t^k, \qquad (4)$$

where the driving process $\boldsymbol{v}_t^k$ is independent and identically distributed (iid) across time t and FP index k and each vector $\boldsymbol{v}_t^k$ is zero-mean Gaussian with a diagonal covariance matrix.

Each FP k is also associated with a random existence variable $e_t^k \in \{0,1\}$, where $e_t^k = 1$ ($e_t^k = 0$) represents the hypothesis that FP k exists (does not exist) at time t. Different e_t^k are assumed to evolve independently according to a first-order Markov chain with FP survival probability $p_{\text{s}} \triangleq \Pr[e_t^k = 1 | e_{t-1}^k = 1] \in [0,1]$ and FP birth probability $\Pr[e_t^k = 1 | e_{t-1}^k = 0] = 0$ [16], [17, Ch. 5]. According to this model, existing FPs can disappear but no new FPs can be created. However, the JIPDA filter includes a heuristic scheme for creating new FPs (see Section IV-E).

B. Measurements

The measurements $\boldsymbol{z}_t(j) \in \mathbb{R}^2$, $j = 1, 2, \ldots, N_t$ are points in Cartesian coordinates. Each $\boldsymbol{z}_t(j)$ is assumed to be associated with a FP $k \in \mathcal{K}_t$ (which is then said to be "detected") or to be clutter (i.e., a false detection caused by imaging artifacts or noise). It is a priori unknown if $\boldsymbol{z}_t(j)$ is associated with any specific FP $k \in \mathcal{K}_t$ or if it is clutter. Each FP can give rise to at most one measurement.

A given FP $k \in \mathcal{K}_t$ is assumed to generate a measurement $\boldsymbol{z}_t(j)$ at time t with a constant "detection probability" $p_{\text{d}} \in [0,1]$. We model the measurement generated by FP k as $\boldsymbol{z}_t(j) = \boldsymbol{y}_t^k + \boldsymbol{w}_t(j)$, where $\boldsymbol{w}_t(j)$ is iid zero-mean Gaussian

measurement noise with covariance matrix $\sigma_w^2\mathbf{I}$. Inserting (1) and (3) results in the nonlinear measurement model

$$\boldsymbol{z}_t(j) = \boldsymbol{c}_t + \phi^{-1}(\boldsymbol{y}_t^{k\star}) + \boldsymbol{w}_t(j) = \boldsymbol{c}_t + \phi^{-1}(\boldsymbol{H}_t\boldsymbol{x}_t^k) + \boldsymbol{w}_t(j).\tag{5}$$

However, since the JIPDA filter assumes a linear measurement model [16], [17, Ch. 5], we linearize (5) as follows. From (5), we have $\boldsymbol{y}_t^{k\star} = \phi(\boldsymbol{z}_t(j) - \boldsymbol{c}_t - \boldsymbol{w}_t(j))$. We approximate the unknown $\boldsymbol{c}_t$ by the previous center point estimate $\hat{\boldsymbol{c}}_{t-1}$ (see (8)), and we approximate the Cartesian-to-polar coordinate mapping $\phi(\boldsymbol{z}) = \left(\sqrt{z_1^2 + z_2^2}\quad \tan^{-1}(z_2/z_1)\right)^{\mathrm{T}}$ by its first-order Taylor series expansion at $\boldsymbol{z}_t(j) - \hat{\boldsymbol{c}}_{t-1}$ [24]. This gives

$$\boldsymbol{y}_t^{k\star} \approx \phi(\boldsymbol{z}_t(j) - \hat{\boldsymbol{c}}_{t-1}) - \boldsymbol{J}_t(j)\boldsymbol{w}_t(j),\tag{6}$$

where $\boldsymbol{J}_t(j)$ is the Jacobian of $\phi(\cdot)$ evaluated at $\boldsymbol{\zeta} \triangleq \boldsymbol{z}_t(j) - \hat{\boldsymbol{c}}_{t-1}$, which is given by $\boldsymbol{J}_t(j) = \begin{pmatrix} \zeta_1/\|\boldsymbol{\zeta}\| & \zeta_2/\|\boldsymbol{\zeta}\| \\ -\zeta_2/\|\boldsymbol{\zeta}\|^2 & \zeta_1/\|\boldsymbol{\zeta}\|^2 \end{pmatrix}$. Writing $\boldsymbol{z}_t^\star(j) \triangleq \phi(\boldsymbol{z}_t(j) - \hat{\boldsymbol{c}}_{t-1})$ for the measurements converted to polar coordinates relative to $\hat{\boldsymbol{c}}_{t-1}$, Eq. (6) reads $\boldsymbol{y}_t^{k\star} \approx \boldsymbol{z}_t^\star(j) - \boldsymbol{J}_t(j)\boldsymbol{w}_t(j)$. Inserting (3) and solving for $\boldsymbol{z}_t^\star(j)$ then yields $\boldsymbol{z}_t^\star(j) \approx \boldsymbol{H}_t\boldsymbol{x}_t^k + \boldsymbol{J}_t(j)\boldsymbol{w}_t(j)$. We thus formally define our *linearized measurement model* as

$$\boldsymbol{z}_t^\star(j) = \boldsymbol{H}_t\boldsymbol{x}_t^k + \boldsymbol{J}_t(j)\boldsymbol{w}_t(j).$$

Clutter measurements (in polar coordinates) are assumed to be distributed according to a homogeneous Poisson point process over the annular search region described in Section II. The mean number of clutter measurements is estimated online using the method described in [17, Sec. 9.3].

IV. CCA Wall Tracking

A. TP Tracking—JIPDA Filter

The core of our CCA wall tracking method is the JIPDA filter [16], [17, Ch. 5], which is a suboptimal Bayes filter that recursively computes relevant FP statistics from all the measurements up to the current time, i.e., $\mathcal{Z}_{1:t}^\star \triangleq (\mathcal{Z}_1^\star, \ldots, \mathcal{Z}_t^\star)$ with $\mathcal{Z}_t^\star \triangleq \{\boldsymbol{z}_t^\star(1), \ldots, \boldsymbol{z}_t^\star(N_t)\}$. The JIPDA filter relies on the linear state-evolution and measurement models discussed in Section III. It uses a Gaussian approximation of the posterior FP state probability density functions $f(\boldsymbol{x}_t^k|e_t^k = 1, \mathcal{Z}_{1:t}^\star)$, $k \in \mathcal{K}_{t-1}$, whose means $\tilde{\boldsymbol{x}}_t^k$ and covariances $\boldsymbol{\Sigma}_t^k$ it calculates time-recursively. In addition, it calculates time-recursively approximations $\hat{p}_t^k$ of the posterior FP existence probabilities $\Pr[e_t^k = 1|\mathcal{Z}_{1:t}^\star]$. Finally, it updates the FP set $\mathcal{K}_{t-1}$ by initializing new FPs and discarding existing FPs with low existence probability (see Section IV-E). This yields the new FP set $\mathcal{K}_t$. The means $\tilde{\boldsymbol{x}}_t^k$ are used as estimates of the FP states $\boldsymbol{x}_t^k$ (see Section IV-B).

We employ a slightly modified version of the JIPDA filter that takes into account the results $\hat{\boldsymbol{c}}_t$ and $\tilde{r}_t$ of the circle parameter estimation stage (see Sections IV-C and IV-D). We will focus on our modifications of the JIPDA filter, since a detailed discussion of the standard JIPDA filter algorithm can be found in [17, Ch. 5].

B. FP Validation

Not all the FPs $k \in \mathcal{K}_{t-1}$ whose statistics were obtained by the JIPDA filter at the previous frame time $t-1$ are good representatives of the CCA wall. The movement of FPs that are far away from the CCA wall may be strongly affected by the inhomogeneity of the tissue surrounding the CCA, and some of the FPs may be altogether due to imaging artifacts. For circle parameter estimation, we therefore use only a subset $\mathcal{K}_{t-1}^{\mathrm{v}} \subseteq \mathcal{K}_{t-1}$ of "valid FPs," which are defined by having both a sufficiently large WAB (see Section IV-F) $\xi_{t-1}^k > \gamma_\xi$ and a sufficiently large posterior existence probability $\hat{p}_t^k > \gamma_p$. Here, the thresholds γ_ξ and γ_p are determined experimentally.

For each valid FP $k \in \mathcal{K}_{t-1}^{\mathrm{v}}$, a position estimate $\tilde{\boldsymbol{y}}_t^k$ (in Cartesian coordinates) is derived from the FP state estimate calculated by the JIPDA filter, $\tilde{\boldsymbol{x}}_t^k$. This is done by using (1) with $\boldsymbol{c}_t$ replaced by $\hat{\boldsymbol{c}}_{t-1}$ and (3) with $\boldsymbol{x}_t^k$ replaced by $\tilde{\boldsymbol{x}}_t^k$, yielding

$$\tilde{\boldsymbol{y}}_t^k = \hat{\boldsymbol{c}}_{t-1} + \phi^{-1}(\boldsymbol{H}_t\tilde{\boldsymbol{x}}_t^k), \quad k \in \mathcal{K}_{t-1}^{\mathrm{v}}.\tag{7}$$

We also calculate a weight $w_t^k \triangleq 1/\lambda_{\max}^k$, where $\lambda_{\max}^k$ denotes the largest eigenvalue of the 2×2 matrix $\boldsymbol{H}_t\boldsymbol{\Sigma}_t^k\boldsymbol{H}_t^{\mathrm{T}}$. We note that $\lambda_{\max}^k$ measures our uncertainty about $\tilde{\boldsymbol{y}}_t^k$, and thus w_t^k is larger for FPs $k \in \mathcal{K}_{t-1}^{\mathrm{v}}$ with a more reliable position estimate.

C. Circle Parameter Estimation

Next, we estimate the CCA circle by fitting a circle to the estimated positions $\tilde{\boldsymbol{y}}_t^k$ of the valid FPs $k \in \mathcal{K}_{t-1}^{\mathrm{v}}$. More specifically, we calculate a CCA center point estimate $\hat{\boldsymbol{c}}_t$ and a CCA radius estimate $\tilde{r}_t$ by minimizing, with respect to $\boldsymbol{c}$ and r, the weighted sum of $(\|\tilde{\boldsymbol{y}}_t^k - \boldsymbol{c}\| - r)^2$, $k \in \mathcal{K}_{t-1}^{\mathrm{v}}$ [25]:

$$(\hat{\boldsymbol{c}}_t, \tilde{r}_t) = \arg\min_{(\boldsymbol{c},r)} \sum_{k \in \mathcal{K}_{t-1}^{\mathrm{v}}} w_t^k (\|\tilde{\boldsymbol{y}}_t^k - \boldsymbol{c}\| - r)^2.\tag{8}$$

This is motivated by the fact that if $\tilde{\boldsymbol{y}}_t^k$ lies on a circle with center point $\boldsymbol{c}$ and radius r, then $\|\tilde{\boldsymbol{y}}_t^k - \boldsymbol{c}\| - r = 0$. In our implementation, the minimization problem (8) is solved numerically by means of the trust-region algorithm [26], which is initialized by $\hat{\boldsymbol{c}}_{t-1}$ and $\tilde{r}_{t-1}$.

According to (8), $\tilde{r}_t$ is calculated separately for each time t, based on the current FP position estimates. This does not directly take advantage of the model (2), (4) describing the radial movement of the CCA wall. Therefore, we next improve the radius estimate $\tilde{r}_t$ by Kalman filtering [17, Ch. 2]. We use $\tilde{r}_t$ as the measurement, and define the measurement model to be (2) with the right-hand side augmented by iid zero-mean Gaussian measurement noise with variance $\sigma_{\tilde{r}}^2$. The state vector is composed of a_t^k, b_t^k, and s_t^k, and its evolution is modeled by a random walk with zero-mean Gaussian driving noise with a diagonal covariance matrix. From the state estimate produced by the Kalman filter, we calculate a radius estimate $\hat{r}_t$ via (2). This is the final result of our method.

D. FP State Estimate Correction

The FP state estimates $\tilde{\boldsymbol{x}}_t^k = \left(\tilde{\boldsymbol{a}}_t^{k\mathrm{T}}\ \tilde{\boldsymbol{b}}_t^{k\mathrm{T}}\ \tilde{s}_t^k\ \tilde{\theta}_t^k\right)^{\mathrm{T}}$ were calculated by the JIPDA filter considering $\hat{\boldsymbol{c}}_{t-1} = \left(\hat{c}_{t-1}^{(1)}\ \hat{c}_{t-1}^{(2)}\right)^{\mathrm{T}}$ as the origin of the coordinate system (see (7)). However, now we

consider the new center point estimate $\hat{\boldsymbol{c}}_t = \left(\hat{c}_t^{(1)} \; \hat{c}_t^{(2)}\right)^{\mathrm{T}}$ as the origin of the coordinate system, and we translate the $\tilde{\boldsymbol{x}}_t^k$ accordingly. The components of the translated FP state estimates $\hat{\boldsymbol{x}}_t^k = \left(\hat{\boldsymbol{a}}_t^{k\mathrm{T}} \; \hat{\boldsymbol{b}}_t^{k\mathrm{T}} \; \hat{s}_t^k \; \hat{\theta}_t^k\right)^{\mathrm{T}}$ are obtained as $\hat{\boldsymbol{a}}_t^k = \tilde{\boldsymbol{a}}_t^k$, $\hat{\boldsymbol{b}}_t^k = \tilde{\boldsymbol{b}}_t^k$, $\hat{s}_t^k = \left(\left(\tilde{s}_t^k \cos(\tilde{\theta}_t^k) + \Delta \hat{c}_t^{(1)}\right)^2 + \left(\tilde{s}_t^k \sin(\tilde{\theta}_t^k) + \Delta \hat{c}_t^{(2)}\right)^2\right)^{1/2}$, and $\hat{\theta}_t^k = \tan^{-1}\left(\frac{\tilde{s}_t^k \sin(\tilde{\theta}_t^k) + \Delta \hat{c}_t^{(2)}}{\tilde{s}_t^k \cos(\tilde{\theta}_t^k) + \Delta \hat{c}_t^{(1)}}\right)$, where $\Delta \hat{c}_t^{(i)} \triangleq \hat{c}_t^{(i)} - \hat{c}_{t-1}^{(i)}$. The $\hat{\boldsymbol{x}}_t^k$ are used to initialize the next JIPDA filter recursion and to calculate the WABs (see Section IV-F).

E. FP Birth/Death Management

After correcting the state estimates, we remove disappeared FPs and initialize newly appeared FPs. FP k is removed from the FP set $\mathcal{K}_{t-1}$ if its posterior existence probability satisfies $\hat{p}_t^k < \gamma_{\mathrm{D}}$. Furthermore, a new FP is initialized for each measurement $\boldsymbol{z}_t^\star(j)$ whose probability of not belonging to any of the current FPs satisfies $P_t(j) > \gamma_{\mathrm{B}}$. Here, $P_t(j) = 1 - \sum_{k \in \mathcal{K}_{t-1}} \hat{p}_t^k \mu_t^k(j)$, where $\mu_t^k(j)$ is an approximation (calculated by the JIPDA filter) of the probability that measurement $\boldsymbol{z}_t^\star(j)$ is associated with FP k, given that $e_t^k = 1$. The thresholds γ_{D} and γ_{B} are determined experimentally. If measurement $\boldsymbol{z}_t^\star(j)$ initializes a new FP k, the corresponding FP state estimate is initialized as $\hat{\boldsymbol{x}}_t^k = \left(\boldsymbol{0}_{2M}^{\mathrm{T}} \; \boldsymbol{z}_t^\star(j)^{\mathrm{T}}\right)^{\mathrm{T}}$ with suitably chosen covariance $\boldsymbol{\Sigma}_t^k = \boldsymbol{\Sigma}_{\mathrm{init}}$ and existence probability $\hat{p}_t^k = p_{\mathrm{init}}$. This process of removing and adding FPs from/to $\mathcal{K}_{t-1}$ defines the new FP set $\mathcal{K}_t$.

F. Calculation of the Wall Association Beliefs

The WABs ξ_{t-1}^k, $k \in \mathcal{K}_{t-1}$ were used in Section IV-B to define the subset $\mathcal{K}_{t-1}^{\mathrm{v}} \subseteq \mathcal{K}_{t-1}$ of "valid FPs" from which the CCA circle parameters are estimated. The WAB $\xi_t^k \in [0, 1]$ quantifies our belief that FP k belongs to the CCA wall. It is defined as follows. Let $\mathcal{T}_t^k \triangleq \{t_{\mathrm{B}}^k, t_{\mathrm{B}}^k + 1, \ldots, t\}$ be the lifetime of FP $k \in \mathcal{K}_t$ up to the current time t; here, t_{B}^k denotes the time when FP k was born. Furthermore, let n_t^k denote the number of times $t' \in \mathcal{T}_t^k$ at which the estimated position $\hat{\boldsymbol{y}}_{t'}^{k\star} \triangleq \boldsymbol{H}_{t'} \hat{\boldsymbol{x}}_{t'}^k$ of FP k was inside an annular region $\mathcal{R}_{t'}$ with center point $\hat{\boldsymbol{c}}_{t'}$, inner radius $\tilde{r}_{t'} - \epsilon$, and outer radius $\tilde{r}_{t'} + \epsilon$, where $\epsilon > 0$ is an experimentally determined constant. (Our definition of $\mathcal{R}_{t'}$ is based on $\tilde{r}_{t'}$ rather than on the Kalman-filtered version $\hat{r}_{t'}$ because $\tilde{r}_{t'}$ is more consistent with the current FP position estimates.) We note that $\hat{\boldsymbol{y}}_{t'}^{k\star}$ is inside $\mathcal{R}_{t'}$ if and only if $|\boldsymbol{h}_{t'} \hat{\boldsymbol{x}}_{t'}^k - \tilde{r}_{t'}| \leq \epsilon$, where $\boldsymbol{h}_{t'}$ is the first row of $\boldsymbol{H}_{t'}$. Finally, let $\alpha_t^k \triangleq n_t^k + \alpha_0^k$ and $\beta_t^k \triangleq \bar{n}_t^k + \beta_0^k$, where $\bar{n}_t^k \triangleq |\mathcal{T}_t^k| - n_t^k$ and the choice of α_0^k and β_0^k is discussed below. Then, the WAB is defined as

$$\xi_t^k \triangleq \frac{\alpha_t^k}{\alpha_t^k + \beta_t^k}, \quad k \in \mathcal{K}_t.$$

We choose α_0^k and β_0^k as follows. For FPs $k \in \mathcal{K}_t$ that exist already at the first frame time, i.e., $t_{\mathrm{B}}^k = 1$, and that initially lie in $\mathcal{R}_1$, i.e., $|\boldsymbol{h}_1 \hat{\boldsymbol{x}}_1^k - \tilde{r}_1| \leq \epsilon$, we set $\alpha_0^k = 10$ and $\beta_0^k = 0$, which results in a high initial WAB $\xi_1^k = \alpha_1^k/(\alpha_1^k + \beta_1^k) = 11/11 = 1$ (note that $n_1^k = 1$ and $\bar{n}_1^k = 0$). This ensures that in the ???transient state of the tracker ???(caused by initialization)

the initial set of FPs is used for circle estimation. A steady state reached in this manner is then likely to follow the actual CCA wall as specified during initialization. For all other FPs— i.e., with $t_{\mathrm{B}}^k > 1$ or with $t_{\mathrm{B}}^k = 1$ but $|\boldsymbol{h}_1 \hat{\boldsymbol{x}}_1^k - \tilde{r}_1| > \epsilon$—we set $\alpha_0^k = \beta_0^k = 1$, which, at the time of birth t_{B}^k, results in $\xi_{t_{\mathrm{B}}^k}^k = 2/3$ (1/3) if FP k is inside (outside) $\mathcal{R}_{t_{\mathrm{B}}^k}$.

V. SIMULATION RESULTS

To demonstrate the performance of our method, we applied it to synthetic CCA ultrasound sequences generated by the Field II ultrasound simulation program [27]. The input to the Field II program is a sequence of sets of scatterers, one set for each frame, and the output is a sequence of ultrasound-like images. At frame time $t = 1$, we randomly generated an initial set of 10^5 scatterers distributed uniformly over the image region. The amplitudes of the scatterers were determined by an echogenicity map, which we created by smoothing and posterizing a real ultrasound image. For each subsequent frame time $t \geq 2$, we generated a new set of scatterers by displacing the scatterers of the initial set according to the mathematical model of CCA wall movement described in [28]. Furthermore, to simulate speckle decorrelation, at each time a specified proportion of scatterers (0%, 2%, or 5%) was replaced by new randomly drawn scatterers. The resulting image sequences— produced by the Field II program—are referred to as S0, S2, and S5, respectively. Each of these sequences consists of 1325 frames. A more detailed description of our generation procedure can be found in [14].

Our JIPDA filter implementation used the belief propagation algorithm proposed in [29] to calculate approximations of the required marginal association probabilities [17, Ch. 5]. The parameters of our model and method were chosen as follows: $\Delta r = 10$, $N_{\max} = 100$, $M = 9$, $\omega = \pi/11$, $p_{\mathrm{s}} = 0.99$, $p_{\mathrm{d}} = 0.5$, $\sigma_w^2 = 5 \cdot 10^{-1}$, $\gamma_\xi = \gamma_p = 0.8$, $\sigma_{\tilde{r}}^2 = 5 \cdot 10^{-1}$, $\gamma_{\mathrm{D}} = 10^{-2}$, $\gamma_{\mathrm{B}} = 0.85$, $\boldsymbol{\Sigma}_{\mathrm{init}} = \mathrm{diag}\{1, \ldots, 1, 1, 0.01\,\mathrm{rad}^2\}$, $p_{\mathrm{init}} = 0.1$, and $\epsilon = 4$. For the driving noise $\boldsymbol{v}_t^k$ (see Section III-A), the variances corresponding to the state components $a_{t,m}^k$ and $b_{t,m}^k$ are $5 \cdot 10^{-2}$, and those corresponding to the state components s_t^k and θ_t^k are $5 \cdot 10^{-1}$ and $10^{-3}\,\mathrm{rad}^2$, respectively. Finally, for the Kalman filter driving noise (see Section IV-C), the variances corresponding to $a_{t,m}^k$ and $b_{t,m}^k$ are 10^{-4}, and the variance corresponding to s_t^k is 10^{-1}.

Table I lists the root-mean-square error (RMSE) of the estimates of the CCA wall displacement obtained with the proposed method and with the reference method of [14]. The CCA wall displacement is defined as the CCA wall circle radius minus its temporal mean [14]. One can see that the proposed method clearly outperforms the reference method for all three scenarios, with an increasing performance advantage for larger speckle decorrelation. For image sequence S5, Fig. 2 shows the estimates of the CCA wall displacement, the true CCA wall displacement, and the absolute value of the estimation error versus time, within a representative time interval. It is seen that the proposed method tends to track the CCA wall radius more accurately than the reference method.

TABLE I
RMSE OF THE CCA WALL DISPLACEMENT ESTIMATES

	RMSE [px]		
	S0	S2	S5
Proposed method	0.4933	0.4095	0.3835
Reference method [14]	0.8256	0.5604	0.6477

VI. CONCLUSION

We explored the use of multitarget tracking for estimating the time-varying radius of the common carotid artery (CCA) from an ultrasound video sequence. Our approach is to track a set of "feature points" (FPs) located around the CCA wall cross section and then fit a circle to the tracked FPs. Our experimental results for simulated ultrasound video sequences demonstrated superior performance of the proposed method relative to a state-of-the-art method. Possible directions for future research include an improvement of the method's robustness to the artifacts and imperfections affecting real ultrasound video sequences and a reduction of the method's sensitivity to the choice of the parameters (thresholds etc.).
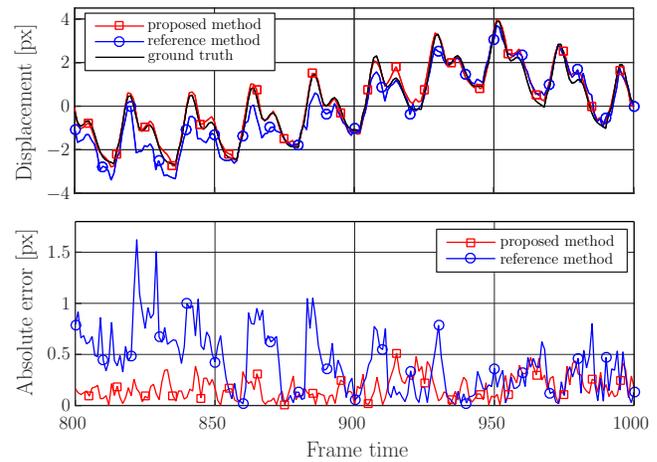

Fig. 2. CCA wall displacement estimates and corresponding estimation errors obtained for S5 with the proposed method and the reference method of [14].

REFERENCES

[1] World Health Organization, "World Health Statistics 2018: Monitoring health for the SDGs," Geneva, Switzerland, 2018.

[2] M. Mokhtari-Dizaji, M. Montazeri, and H. Saberi, "Differentiation of mild and severe stenosis with motion estimation in ultrasound images," *Ultrasound Med. Biol.*, vol. 32, no. 10, pp. 1493–1498, Oct. 2006.

[3] Z. Gao, Y. Li, Y. Sun, J. Yang, H. Xiong, H. Zhang, X. Liu, W. Wu, D. Liang, and S. Li, "Motion tracking of the carotid artery wall from ultrasound image sequences: A nonlinear state-space approach," *IEEE Trans. Med. Imag.*, vol. 37, no. 1, pp. 273–283, Jan. 2017.

[4] E. J. Chen, R. S. Adler, P. L. Carson, W. K. Jenkins, and W. D. O'Brien, "Ultrasound tissue displacement imaging with application to breast cancer," *Ultrasound Med. Biol.*, vol. 21, no. 9, pp. 1153–1162, Jan. 1995.

[5] S. Golemati, A. Sassano, M. J. Lever, A. A. Bharath, S. Dhanjil, and A. N. Nicolaides, "Carotid artery wall motion estimated from B-mode ultrasound using region tracking and block matching," *Ultrasound Med. Biol.*, vol. 29, no. 3, pp. 387–399, Mar. 2003.

[6] J. Tat, J. S. Au, P. J. Keir, and M. J. MacDonald, "Reduced common carotid artery longitudinal wall motion and intramural shear strain in individuals with elevated cardiovascular disease risk using speckle tracking," *Clin. Physiol. Funct. Imag.*, vol. 37, no. 2, pp. 106–116, Mar. 2017.

[7] A. Gastounioti, S. Golemati, J. Stoitsis, and K. Nikita, "Kalman-filter-based block matching for arterial wall motion estimation from B-mode ultrasound," in *Proc. IEEE Int. Conf. Imag. Syst. Techn.*, Thessaloniki, Greece, Jul. 2010, pp. 234–239.

[8] G. Zahnd, M. Orkisz, A. Sérusclat, P. Moulin, and D. Vray, "Evaluation of a Kalman-based block matching method to assess the bi-dimensional motion of the carotid artery wall in B-mode ultrasound sequences," *Med. Image Anal.*, vol. 17, no. 5, pp. 573–585, Jul. 2013.

[9] A. Gastounioti, S. Golemati, J. Stoitsis, and K. S. Nikita, "Comparison of Kalman-filter-based approaches for block matching in arterial wall motion analysis from B-mode ultrasound," *Meas. Sci. Technol.*, vol. 22, no. 11, pp. 1–9, Oct. 2011.

[10] B. D. Lucas and T. Kanade, "An iterative image registration technique with an application to stereo vision," in *Proc. Int. Joint Conf. Artif. Intell.*, Vancouver, BC, Canada, Aug. 1981, pp. 674–679.

[11] K. Říha and I. Potůček, "The sequential detection of artery sectional area using optical flow technique," in *Proc. WSEAS Int. Conf. Circ. Syst. Electron. Contr. Signal Process.*, Stevens Point, WI, USA, Dec. 2009, pp. 222–226.

[12] A. Gastounioti, N. N. Tsiaparas, S. Golemati, J. S. Stoitsis, and K. S. Nikita, "Affine optical flow combined with multiscale image analysis for motion estimation of the arterial wall from B-mode ultrasound," in *Proc. Ann. Int. Conf. IEEE Eng. Med. Biol. Soc.*, Boston, MA, USA, Aug. 2011, pp. 559–562.

[13] S. Golemati, J. S. Stoitsis, A. Gastounioti, A. C. Dimopoulos, V. Koropouli, and K. S. Nikita, "Comparison of block matching and differential methods for motion analysis of the carotid artery wall from ultrasound images," *IEEE Trans. Inf. Technol. Biomed.*, vol. 16, no. 5, pp. 852–858, Sep. 2012.

[14] K. Říha, M. Zukal, and F. Hlawatsch, "Analysis of carotid artery transverse sections in long ultrasound video sequences," *Ultrasound Med. Biol.*, vol. 44, no. 1, pp. 153–167, Jan. 2018.

[15] Y. Bar-Shalom and T. E. Fortmann, *Tracking and Data Association*. Orlando, FL, USA: Academic Press, 1988.

[16] D. Mušicki and R. Evans, "Joint integrated probabilistic data association – JIPDA," in *Proc. FUSION 2002*, Annapolis, MD, USA, Jul. 2002, pp. 1120–1125.

[17] S. Challa, M. R. Morelande, D. Mušicki, and R. J. Evans, *Fundamentals of Object Tracking*. Cambridge, UK: Cambridge University Press, 2011.

[18] K. Říha, J. Mašek, R. Burget, R. Beneš, and E. Závodná, "Novel method for localization of common carotid artery transverse section in ultrasound images using modified Viola-Jones detector," *Ultrasound Med. Biol.*, vol. 39, no. 10, pp. 1887–1902, Oct. 2013.

[19] R. O. Duda and P. E. Hart, "Use of the Hough transformation to detect lines and curves in pictures," *Commun. ACM*, vol. 15, no. 1, pp. 11–15, Jan. 1972.

[20] C. Harris and M. Stephens, "A combined corner and edge detector," in *Proc. Alvey Vision Conf.*, Manchester, UK, Aug. 1988, pp. 147–152.

[21] T. L. Szabo, *Diagnostic Ultrasound Imaging: Inside Out*, 2nd ed. Amsterdam, The Netherlands: Academic Press, 2014.

[22] W. Nichols, M. O'Rourke, and C. Vlachopoulos, *McDonald's Blood Flow in Arteries: Theoretical, Experimental and Clinical Principles*, 6th ed. London, UK: CRC Press, 2011.

[23] S. Kim, A. S. Paul, E. A. Wan, and J. McNames, "Multiharmonic tracking using sigma-point Kalman filter," in *Proc. Ann. Int. Conf. IEEE Eng. Med. Biol. Soc.*, Vancouver, Canada, Aug. 2008, pp. 2648–2652.

[24] X. R. Li and V. P. Jilkov, "Survey of maneuvering target tracking. Part III: Measurement models," in *SPIE Proc. Vol. 4473: Signal and Data Processing of Small Targets*, Nov. 2001.

[25] I. D. Coope, "Circle fitting by linear and nonlinear least squares," *J. Opt. Theory Appl.*, vol. 76, no. 2, pp. 381–388, Feb. 1993.

[26] T. F. Coleman and Y. Li, "An interior trust region approach for nonlinear minimization subject to bounds," *SIAM J. Opt.*, vol. 6, no. 2, pp. 418–445, Jul. 1996.

[27] J. A. Jensen, "Field: A program for simulating ultrasound systems," *Med. Biol. Eng. Comput.*, vol. 34, no. sup. 1, pp. 351–353, Jan. 1997.

[28] J. Stoitsis, S. Golemati, E. Bastouni, and K. S. Nikita, "A mathematical model of the mechanical deformation of the carotid artery wall and its application to clinical data," in *Proc. Ann. Int. Conf. IEEE Eng. Med. Biol. Soc.*, Lyon, France, Aug. 2007, pp. 2163–2166.

[29] J. Williams and R. Lau, "Approximate evaluation of marginal association probabilities with belief propagation," *IEEE Trans. Aerosp. Electron. Syst.*, vol. 50, no. 4, pp. 2942–2959, Oct. 2014.